Phase transitions between Reissner-Nordstrom and dilatonic black holes in 4D AdS spacetime

Mariano Cadoni,* Giuseppe D'Appollonio,† and Paolo Pani‡
Dipartimento di Fisica, Università di Cagliari and INFN, Sezione di Cagliari

We study Einstein-Maxwell-dilaton gravity models in four-dimensional anti-de Sitter (AdS) spacetime which admit the Reissner-Nordstrom (RN) black hole solution. We show that below a critical temperature the AdS-RN solution becomes unstable against scalar perturbations and the gravitational system undergoes a phase transition. We show using numerical calculations that the new phase is a charged dilatonic black hole. Using the AdS/CFT correspondence we discuss the phase transition in the dual field theory both for non-vanishing temperatures and in the extremal limit. The extremal solution has a Lifshitz scaling symmetry. We discuss the optical conductivity in the new dual phase and find interesting behavior at low frequencies where it shows a "Drude peak". The resistivity varies with temperature in a non-monotonic way and displays a minimum at low temperatures which is reminiscent of the celebrated Kondo effect.

I. INTRODUCTION

The AdS/CFT correspondence [1] provides a deep connection between quantum gravity and quantum gauge theories. When the classical gravity approximation is reliable, it also provides efficient techniques for the computation of the thermodynamical and transport properties of strongly interacting quantum field theories. This holographic approach has been applied both to gauge theories similar to QCD [2, 3] and, more recently, to condensed matter phenomena [4–7]. It relies on the identification between the black hole solutions of the bulk theory and the thermal states of the boundary theory. Transport coefficients can be computed at strong coupling by solving the equations governing small perturbations of the black hole background [8].

In the attempt of developing a gravitational description for condensed matter phenomena one is primarily interested in finding black hole solutions that can capture the salient features of realistic many-body systems and in studying the corresponding phase diagram. The existence and the stability properties of a given solution depend on the field content and on the couplings of the bulk action. As an illustration of this point let us consider the simplest example, relevant for the holographic description of systems at finite temperature and charge density. The minimal bulk theory is in this case Einstein-Maxwell theory and the only static charged black hole solution is the AdS-Reissner-Nordström (AdS-RN) black hole [9]. The solution remains stable as we lower the temperature and the ground state of the system corresponds to the extremal AdS-RN black hole. If we include in the action a charged scalar field with a minimal coupling to the gauge field, below a critical temperature new branches of solutions appear which are thermodynamically favoured. The resulting instability of the AdS-RN black hole provides a holographic description of a phase transition in the dual theory [10–12]. Below the critical temperature the new solution is a static charged black hole with a scalar hair. The non-trivial profile of the scalar field corresponds to a charged condensate in the dual theory that breaks spontaneously a global $U(1)$ symmetry. One then expects to observe in the new phase phenomena typical of superfluid or superconducting systems and this is confirmed by the study of the linearized response of the hairy black hole to small perturbations [11, 12].

Most investigations considered so far only the case of scalar fields minimally coupled to the electromagnetic field. Relatively little is known about the stability of the AdS-RN solution in non-minimally coupled models (Einstein-Maxwell-dilaton gravity). Non-minimal couplings of the form $f(\phi)F^2$ between a scalar fields ϕ and the Maxwell tensor are very common in supergravity and in the low-energy effective action of string theory models. In flat spacetime charged black holes solutions of Einstein-Maxwell-dilaton gravity are well-known [13–15]. These solutions involve a non-constant scalar field and differ significantly from the RN black hole since there is no inner horizon and the event horizon becomes singular in the extremal limit. Examples of charged dilaton black hole solutions with AdS asymptotics are provided by the family of four-charge black holes in $\mathcal{N} = 8$ four-dimensional gauged supergravity [16]. As shown in [17] in the extremal limit these black holes can support an isolated fermion normal mode which signals

*Electronic address: email:mariano.cadoni@ca.infn.it
†Electronic address: email:giuseppe.dappollonio@ca.infn.it
‡Electronic address: email:paolo.pani@ca.infn.it

the presence of a Fermi surface in the dual systems. Quite interestingly the AdS-RN black hole is not a solution of dilaton gravity models with $f = \exp(a\phi)$.

In this paper we shall consider models where the coupling between the scalar field and the kinetic term of the gauge field starts quadratically. We first investigate the stability of the AdS-RN black hole under scalar perturbations and show that it becomes unstable below a critical temperature. In flat space this kind of instability was studied in [18]. In [19] it was found that the AdS-RN black hole in $\mathcal{N} = 8$ four-dimensional gauged supergravity is unstable against fluctuations involving a scalar and four gauge fields. In [20] a similar instability was found studying scalar fluctuations around a dyonic black hole in order to compute the momentum relaxation time scale induced by the presence of impurities.

In our models AdS-RN and dilaton black holes can coexist. Below a critical temperature the AdS-RN solution undergoes a phase transition toward a new solution, which is a hairy black hole solution. Following closely the approach of [11, 12] we will construct numerically the hairy black hole solutions. In order to clarify the behavior of the model at low temperatures we will also study the extremal solution. The near horizon form is characterized by a Lifshitz scaling isometry [21] and is a simple generalization of the solution found in [22].

In the new phase a neutral scalar operator acquires a non-vanishing expectation value. The condensate modifies the transport properties of the system in an interesting way. This is clearly illustrated by the behavior we find for the optical conductivity at small frequencies and non-vanishing temperatures: there is a minimum and then the conductivity increases until it reaches a value which can be much higher than the constant value at high frequencies. We can understand this fact by rewriting the equation for the vector fluctuations as a Schrödinger equation [23]. The non-minimal coupling between the scalar and the gauge field induces a term in the potential that is not positive definite. A similar behavior was recently observed in models where the Born-Infeld action of a probe brane is coupled to a geometry with a Lifshitz scaling symmetry [24].

Another interesting feature of the new phase is the fact that the resistivity does not increase monotonically with the temperature but displays a minimum. A similar behavior of the resistivity is observed in metals containing magnetic impurities, an effect explained by Kondo as resulting from the interaction between the magnetic moment of the conduction electrons and the impurity.

The plan of this paper is as follows. In Section II we present our model and discuss the stability of the AdS-RN black hole against scalar perturbations, providing approximate criteria to identify the region in parameter space where an instability is likely to occur. In Section III we construct numerically the charged black hole solutions with a neutral scalar hair and show that they are thermodynamically favoured. In Sec. IV we give the analytic form of the near-horizon solution for the extremal and near-extremal black holes. In Section V we analyze the optical conductivity in the new phase of the dual field theory described by the dilaton black hole. In Sec. VI we present our conclusions.

II. INSTABILITY OF ADS-RN BLACK HOLES IN EINSTEIN-MAXWELL-DILATON GRAVITY

In this paper we consider Einstein gravity coupled to an abelian gauge field A_μ and a real scalar field ϕ. The Lagrangian

$$\mathcal{L} = R - \frac{f(\phi)}{4}F^2 - \frac{1}{2}\partial^\mu\phi\partial_\mu\phi - V(\phi)\,, \tag{2.1}$$

depends on the choice of two functions, a potential $V(\phi)$ and a function $f(\phi)$ that couples the scalar to the kinetic term of the gauge field. Lagrangians of this type are common in supergravity and in the low-energy limit of string theory models. The equations of motion read

$$\begin{aligned}
&\nabla_\mu\left(f(\phi)F^{\mu\nu}\right) = 0\,,\\
&\nabla^2\phi = \frac{dV(\phi)}{d\phi} + \frac{df(\phi)}{d\phi}\frac{F^2}{4}\,,\\
&R_{\mu\nu} - \frac{1}{2}g_{\mu\nu}R = -\frac{f(\phi)}{2}\left(F_{\mu\rho}F^{\rho}{}_{\nu} + \frac{g_{\mu\nu}}{4}F^{\rho\sigma}F_{\rho\sigma}\right) + \frac{1}{2}\left(\partial_\mu\phi\partial_\nu\phi - \frac{g_{\mu\nu}}{2}\partial^\rho\phi\partial_\rho\phi\right) - \frac{g_{\mu\nu}}{2}V(\phi)\,.
\end{aligned} \tag{2.2}$$

We shall restrict the possible choices of $V(\phi)$ and $f(\phi)$ by imposing two requirements. The first is that the potential $V(\phi)$ admits stable AdS vacua. Assuming for simplicity that there is only one extremum at $\phi = 0$, the potential can be expanded for small values of the field as

$$V(\phi) = -\frac{6}{L^2} + \frac{\beta}{2L^2}\phi^2 + \mathcal{O}(\phi^3)\,, \tag{2.3}$$

where L is the AdS radius and β parametrizes the mass of the field, $m^2L^2 = \beta$. The AdS vacuum is stable if the mass parameter satisfies the Breitenlohner-Freedman (BF) bound $\beta \geq -9/4$ [25]. In the following we will limit our discussion to quadratic potentials and to potentials of the form $V(\phi) = -2W_0 \cosh(b\phi)$. In the latter case $L^2 = 3/W_0$, $\beta = -6b^2$ and the BF bound becomes $b^2 \leq 3/8$.

The second requirement is that the AdS-RN black hole is a solution of the equations (2.2). This is the case if the first derivative of the coupling function vanishes at the extremum of V, $\frac{df}{d\phi}(0) = 0$. For small values of the field the function f can be expanded as

$$f(\phi) = 1 + \frac{\alpha}{2}\phi^2 + \mathcal{O}(\phi^3)\,, \tag{2.4}$$

where the parameter α is assumed to be non-negative. In the following we will consider mainly quadratic coupling functions and functions of the form $f(\phi) = \cosh(a\phi)$ for which $\alpha = a^2$. In our analysis of the zero temperature limit of the hairy black hole solutions in Section IV we will also consider exponential coupling functions.

We will look for static electrically charged solutions of the equations of motion with translational symmetry in two spatial directions. The metric can be written as

$$ds^2 = -g(r)e^{-\chi(r)}dt^2 + \frac{dr^2}{g(r)} + r^2(dx^2 + dy^2)\,. \tag{2.5}$$

The scalar field is $\phi = \phi(r)$ and only the temporal component of the gauge potential is non-vanishing, $A_0 = A_0(r)$. The equations of motion become

$$\phi'' + \left(\frac{g'}{g} - \frac{\chi'}{2} + \frac{2}{r}\right)\phi'(r) - \frac{1}{g}\frac{dV}{d\phi} + \frac{{A_0'}^2 e^{\chi}}{2g}\frac{df}{d\phi} = 0\,, \tag{2.6}$$

$$(r^2 e^{\frac{\chi}{2}} f(\phi) A_0')' = 0\,, \tag{2.7}$$

$$\chi' + \frac{r{\phi'}^2}{2} = 0\,, \tag{2.8}$$

$$\frac{{\phi'}^2}{4} + \frac{{A_0'}^2 e^{\chi} f(\phi)}{4g} + \frac{g'}{rg} + \frac{1}{r^2} + \frac{V(\phi)}{2g} = 0\,, \tag{2.9}$$

where here and in the following a prime will always denote a derivative with respect to r. When the condition (2.4) is satisfied, the equations of motion admit the AdS-RN black hole solution

$$g = -\frac{2M}{r} + \frac{Q^2}{4r^2} + \frac{r^2}{L^2}\,, \qquad \chi = 0\,, \qquad A_0 = \frac{Q}{r} - \frac{Q}{r_h}\,, \qquad \phi = 0\,, \tag{2.10}$$

where M and Q are respectively the mass and the electric charge of the black hole and r_h the radius of the horizon. The black hole temperature is

$$4\pi T_{RN} = \frac{3r_h}{L^2} - \frac{Q^2}{4r_h^3}\,, \tag{2.11}$$

and the solution becomes extremal for $12r_h^4 = Q^2L^2$.

Let us now discuss the stability of the AdS-RN solution (2.10) against small perturbations of the scalar field. Given the planar symmetry of the solution, we can expand the scalar perturbation in Fourier modes

$$\phi_{\omega,\vec{k}} = \frac{R(r)}{r} e^{i(k_1 x + k_2 y - \omega t)}\,. \tag{2.12}$$

The radial function R solves the following equation

$$g^2 R'' + gg' R' + \left[\omega^2 - V\right] R = 0\,, \qquad V = g\left[\frac{\vec{k}^2}{r^2} + \frac{g'}{r} + m_{\rm eff}^2\right]\,, \tag{2.13}$$

where we have introduced an effective mass

$$m_{\rm eff}^2(r) = m^2 - \frac{\alpha}{2}A_0'(r)^2\,. \tag{2.14}$$

In the presence of an electric background field the non-minimal coupling gives a negative contribution to the effective mass. If the coupling is strong enough it can lower the mass below the BF bound and destabilize the background. This mechanism of instability can be generalized to magnetic and dyonic black holes. In this case whether the solution is stable or unstable depends on the sign of the coupling α and on the relative magnitude of the electric and magnetic charges. In flat space this kind of instability was studied in [18]. In [19] a dynamical instability of the AdS-RN black hole in $\mathcal{N}=8$ four-dimensional gauged supergravity was found involving fluctuations of both scalar and gauge fields. A similar instability was also found in [20] analysing scalar fluctuations around a dyonic black hole in order to compute the momentum relaxation time scale induced by the presence of impurities.

Before studying numerically the solutions of Eq. (2.13), it is worth discussing some approximate criteria that point to the instability of the AdS-RN background. When $\beta=-2$ we can in fact provide a simple proof of the instability. In this case the potential $V(r)$ vanishes both at the horizon and at infinity and a sufficient condition for the existence of unstable modes is given by [26]

$$\int_{r_h}^{\infty} dr \frac{V(r)}{g(r)} < 0\,. \tag{2.15}$$

In terms of the parameter α this instability condition becomes

$$\alpha > \frac{3r_h^4}{Q^2L^2} - \frac{1}{4}\,. \tag{2.16}$$

For generic values of β an approximate condition for the instability of the solution follows from the observation that the region where the effective mass is below the BF bound contributes to the formation of a tachyonic mode whereas the region where the effective mass is above the BF bound supports stability. We can characterize the two regions introducing an instability radius r_i

$$r_i^4 = \frac{Q^2L^2}{\gamma}\,, \qquad \gamma = \frac{2}{\alpha}\left(\frac{9}{4}+\beta\right)\,. \tag{2.17}$$

The region where $m^2_{\text{eff}} < -9/4$ corresponds to $r < r_i$ while the region where $m^2_{\text{eff}} > -9/4$ corresponds to $r > r_i$. When $r_i \gg r_h$ the AdS-RN black hole is likely to be unstable and since $r_i \to \infty$ when $\alpha \to \infty$ or when $\beta \to -9/4$ we expect an instability for large values of α or for masses close to the BF bound. This approximate condition can be expressed in terms of the black hole temperature (2.11) as

$$T_i \gg T_{RN}\,, \qquad T_i = \frac{\sqrt{QL}}{16\pi L^2}\left(\frac{12-\gamma}{\gamma^{1/4}}\right)\,. \tag{2.18}$$

The instability temperature is shown in Figure 1 as a function of the black hole charge Q. The region where an instability is expected to occur is $T_{RN} \ll T_i$, i.e. $Q \gg Q_i$, where Q_i is given by the intersection point of the two curves $T_{RN}(Q)$ and $T_i(Q)$.

In order to confirm the existence of the instability one should find unstable modes of the scalar equation (2.13). Unstable modes correspond to normalizable solutions of (2.13) with purely ingoing boundary conditions at the horizon and complex frequency ω with $\text{Im}(\omega) > 0$ (see [27] for a recent review on black hole perturbations). These modes grow exponentially in time destabilizing the background. Another strong indication of the instability of a gravitational background is provided by the presence of marginally stable modes, namely modes with $\omega = 0$. Setting also $\vec{k}=0$, Eq. (2.13) reduces to

$$\left(\Box - m^2_{\text{eff}}\right)\phi(r) = 0\,. \tag{2.19}$$

We can solve the previous equation by numerical integration starting from a series expansion at the horizon and imposing suitable boundary conditions near the AdS boundary. The expansion at large r of the scalar field is

$$\phi \sim \frac{\mathcal{O}_\Delta}{r^\Delta}\,, \tag{2.20}$$

with $\Delta(\Delta-3) = m^2$ and Δ chosen in such a way that the scalar mode is normalizable. We solve Eq. (2.19) numerically fixing α and β and varying L until we find a solution with the correct asymptotic behavior (2.20). A solution exists for $L \leq 2\sqrt{3}$ and as we increase L to lower the temperature several marginally stable modes arise. Some examples of marginal modes are shown in Figure 2 and 3.

The numerical results confirm the qualitative discussion at the beginning of this Section. The instability temperature (2.18) provides a good estimate of the critical temperature at which the first marginal mode actually appears, it

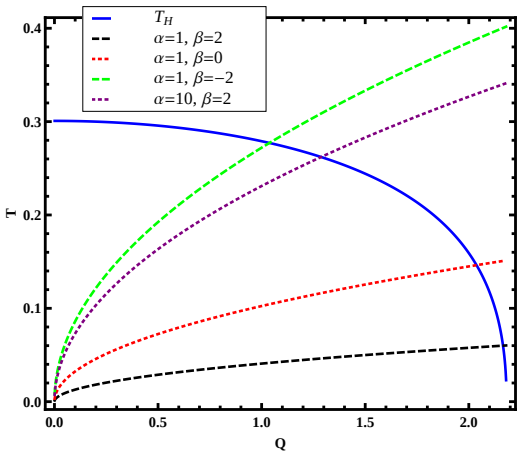

FIG. 1: The instability temperature T_i and the black hole temperature T_{RN} as functions of Q for $L = M = 1$. Plots extend from $Q = 0$ to $Q_{\rm ext} = M\sqrt{3}(2L/M)^{1/3}$ which corresponds to extremal black holes. The region of instability is $T_{RN} \ll T_i$. Curves are ordered in a counterclockwise sense for decreasing values of γ. The smaller γ the larger the instability region.

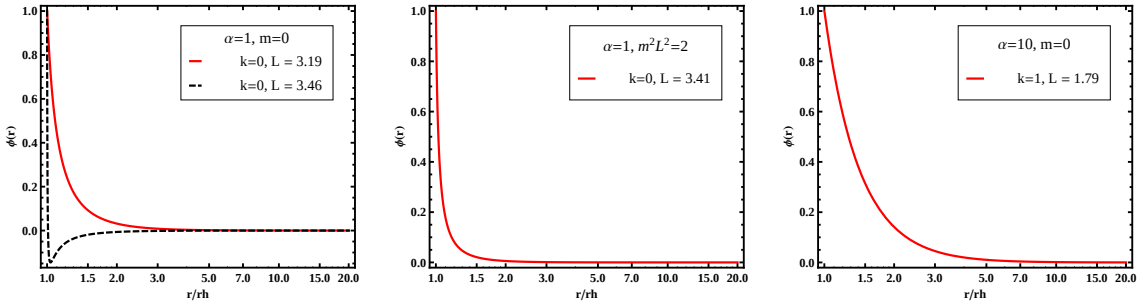

FIG. 2: Some examples of marginally stable modes with $m^2 \geq 0$

overestimates the numerical value by a factor of order one which decreases in the large α limit. Marginal modes appear in a large region of the parameter space and they provide a strong indication of the instability of the AdS-RN black hole.

Finally integrating numerically Eq. (2.13) with $\omega \neq 0$ we found quasinormal modes with $\mathrm{Im}(\omega) > 0$, which provide the main indication for the existence of a dynamical instability. As expected the imaginary part of the frequency of these unstable modes increases as we increase α or consider values of β close to the BF bound.

III. NUMERICAL SOLUTIONS OF THE FIELD EQUATIONS

The existence of a perturbative instability for the AdS-RN black hole in models containing a scalar field with a non-minimal coupling to the gauge field suggests that the Lagrangian (2.1) should admit charged dilaton black holes with $T \leq T_c$ and a lower free energy than the AdS-RN black hole. In this Section we show that these solutions exist by solving numerically the full nonlinear equations of motion (2.2). In Appendix A we discuss a simpler probe limit in which the stress-energy tensors of the Maxwell and of the scalar field decouple from the Einstein equations.

Analytic solutions for static, charged, planar black holes with scalar hairs are difficult to find. Charged black holes with a scalar hair in a similar model were found in flat spacetime [15] and their generalization to AdS spacetime were considered recently in [28]. The asymptotic behavior of the scalar field is however not the one required for the study of phase transitions in the dual theory. In [29] numerical black hole solutions with a scalar hair were found in flat space for models of dilaton gravity coupled to the Born-Infeld action. Charged black hole solutions with scalar hairs in AdS were only found resorting to numerical computations [11, 30] and we shall follow the same approach here.

To set up the numerical procedure we first consider the behavior of the fields near the AdS boundary for $r \to \infty$

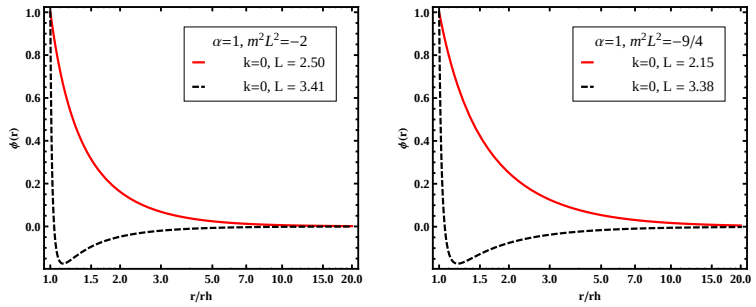

FIG. 3: Some examples of marginally stable modes with $0 \geq m^2 \geq m^2_{BF}$

and near the horizon for $r \to r_h$. The asymptotic behavior near the AdS boundary of the scalar field is

$$\phi \sim \frac{\mathcal{O}_-}{r^{\Delta_-}} + \frac{\mathcal{O}_+}{r^{\Delta_+}} , \tag{3.1}$$

where

$$\Delta_\pm = \frac{3 \pm \sqrt{9 + 4m^2L^2}}{2} . \tag{3.2}$$

In order to describe states of the dual field theory with a non vanishing expectation value for the operator dual to the scalar field, the asymptotic expansion (3.1) should contain only normalizable modes [31]. For this reason when $m^2L^2 \geq -5/4$ we impose the boundary condition $\mathcal{O}_- = 0$, corresponding to a vacuum expectation value for an operator of dimension Δ_+. When $-9/4 < m^2L^2 < -5/4$ two distinct choices are possible [32]: $\mathcal{O}_- = 0$, corresponding to a vacuum expectation value for an operator of dimension Δ_+ and $\mathcal{O}_+ = 0$, corresponding to a vacuum expectation value for an operator of dimension Δ_-.

The asymptotic behavior of the gauge field is

$$A_0 \sim \mu - \frac{\rho}{r} , \tag{3.3}$$

where μ and ρ specify the chemical potential and the charge density of the dual theory [6]. Finally the asymptotic behavior of the metric functions is given by

$$\chi \sim \frac{\Delta \mathcal{O}_\Delta^2}{4L^2} \frac{1}{r^{2\Delta}} , \tag{3.4}$$

and

$$\begin{aligned} g &\sim \frac{r^2}{L^2} + \frac{\Delta \mathcal{O}_\Delta^2}{4L^2} \frac{1}{r^{2\Delta-2}} - \frac{2M}{r} , && \text{if } 1 < 2\Delta \leq 2 , \\ g &\sim \frac{r^2}{L^2} - \frac{2M}{r} , && \text{if } \Delta > 1 , \end{aligned} \tag{3.5}$$

where M is the black hole mass. Asymptotically the solution is then characterized by four parameters: μ, ρ, M and $\mathcal{O}_\Delta$.

A power series expansion near the horizon shows that the solutions of the equations (2.6)-(2.9) are completely specified by four parameters [11]: the horizon radius r_h, $A_0'(r_h)$, $\chi(r_h) \equiv \chi_h$ and $\phi(r_h) \equiv \phi_h$. In term of these parameters the black hole temperature is

$$T = \frac{r_h}{16\pi L^2} \left[(12 + 2\phi_h^2) e^{-\chi_h/2} - L^2 A_0'(r_h)^2 e^{\chi_h/2} f(\phi_h) \right] . \tag{3.6}$$

In order to reduce the number of parameters in the numerical analysis one can exploit the following three scaling symmetries of the equations of motion [12]

$$\begin{aligned} & r \mapsto kr , \quad t \mapsto kt , \quad L \mapsto kL , \\ & r \mapsto kr , \quad (t,x,y) \mapsto \frac{1}{k}(t,x,y) , \quad g \mapsto k^2 g , \quad A_0 \mapsto k A_0 , \\ & t \mapsto kt , \quad e^\chi \mapsto k^2 e^\chi , \quad A_0 \mapsto \frac{1}{k} A_0 . \end{aligned} \tag{3.7}$$

We can use the first symmetry to set $L = 1$, the second to set $r_h = 1$ (assuming that the horizon radius is different from zero) and the third to set to zero the asymptotic value of χ at infinity. In this way we are left with two parameters, ϕ_h and $A_0'(r_h)$, that are constrained by the condition that either $\mathcal{O}_+$ or $\mathcal{O}_-$ vanish at infinity. It follows that the numerical solutions of the field equations (2.6)-(2.9) form a one-parameter family. Varying the single free parameter, e.g. ϕ_h, one obtains solutions with different values of the temperature (3.6).

By numerical integration we found solutions of the field equations (2.6)-(2.9) that describe charged dilatonic black holes. We considered two types of coupling functions

$$f_1(\phi) = \cosh(a\phi) \ , \qquad\qquad f_2(\phi) = 1 + \frac{\alpha}{2}\phi^2 \ , \tag{3.8}$$

and two types of potentials

$$V_1(\phi) = -\frac{6}{L^2} + \frac{\beta}{2L^2}\phi^2 \ , \qquad\qquad V_2(\phi) = -\frac{6}{L^2}\cosh(b\phi) \ . \tag{3.9}$$

In Figure 4 we display the field profiles of the numerical solution obtained for a particular choice of f and V. Other choices lead to qualitatively similar results.

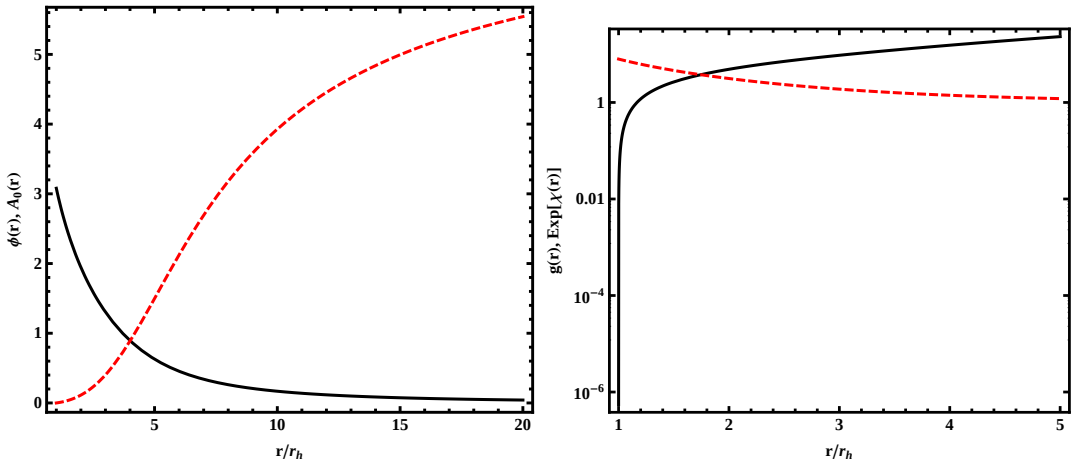

FIG. 4: Examples of the field profiles of the numerical charged black hole solution for a coupling function $f(\phi) = \cosh(2\phi)$ and a potential $L^2V(\phi) = -6 - \phi^2$. Left panel: the scalar field ϕ (black) and the gauge potential A_0 (dashed red). Right panel: metric function g (black) and e^χ (dashed red). $T/T_c \sim 0.2$.

Below a critical temperature $T_c \sim \sqrt{\rho}$ we always find charged dilaton black hole solutions. Comparing their free energy with the free energy of the AdS-RN one can verify that they represent more stable states. The free energy $F = M - TS - \Phi Q$ depends on the four asymptotic parameters that characterize the solution, namely μ, ρ, M and $\mathcal{O}_\Delta$. Setting $L = 1$ the free energies of the AdS-RN black hole and of the dilaton black hole read [11]

$$F_{RN} = \frac{V}{r_h}\left(-r_h^4 + \frac{3\rho^2}{4}\right) \ , \qquad\qquad F_{CD} = V\left(-2M + \mu\rho\right) \ , \tag{3.10}$$

where V is the volume of the (x, y) plane. In Fig. 5 we plot the free energy and the specific heat $c = -T\partial_T^2 F/V$ for an AdS-RN black hole and a charged dilatonic black hole with the same mass and charge. Below T_c the dressed solution has a lower free energy and represents a more stable state than the AdS-RN black hole. The free energy is continuous at T_c while the specific heat has a discontinuity, so that the phase transition is second order. For $T > T_c$ the dressed solution is not present anymore, precisely as it happens for the instability induced by the minimal coupling to a charged scalar field [12, 33]. We mention here that for a given choice of f and V there are usually several different black hole solutions with scalar hair and the correct asymptotic behavior. We always choose the solution with a monotonic scalar profile. The other solutions have scalar fields with several nodes and presumably they also have a higher free energy.

IV. THE ZERO TEMPERATURE LIMIT

Below the critical temperature the gravitational background describes a charged dilaton black hole. In this section we discuss the properties of the zero temperature ground state. Extremal solutions are not easily found numerically.

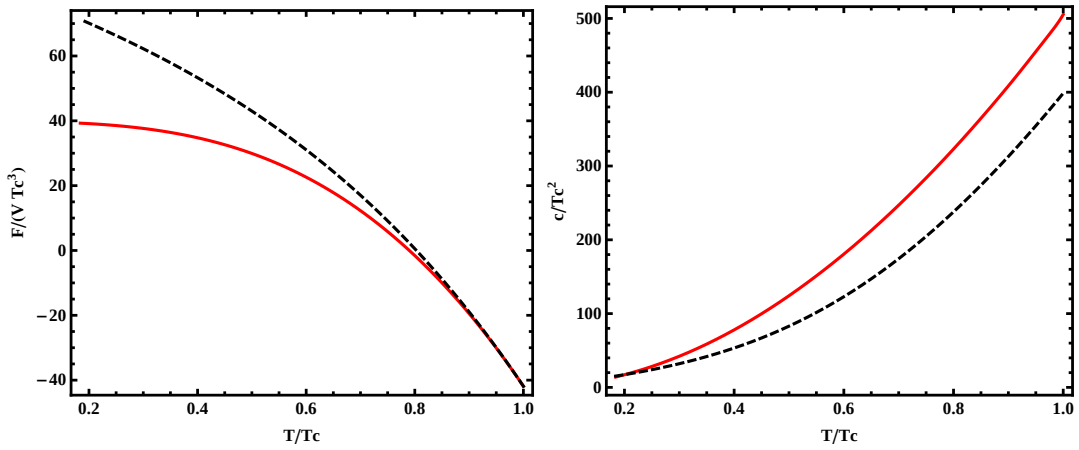

FIG. 5: Left panel: Free energy of the hairy black hole (red line) and of the AdS-RN (black dashed line). Right panel: specific heat. The data shown are for the operator $\mathcal{O}_-$ and for $f(\phi) = \cosh(2\phi)$ and $V(\phi) = -6/L^2 - \phi^2/L^2$.

In order to study their properties one can first look for an ansatz for the leading behavior of the fields near the horizon that contains at least one free parameter. The equations of motion are then integrated numerically and the free parameter varied until one finds the correct asymptotic behavior at infinity. In this way a solution to the equations of motion with the correct boundary conditions is obtained [23]. The zero temperature limit of hairy black holes in models with a minimally coupled charged scalar field was studied in [23]. In [22] a similar analysis was carried out for dilaton black holes with an exponential coupling function $f(\phi) = e^{a\phi}$.

We limit our attention to models with coupling function and potential of the form

$$f(\phi) = 2f_0 \cosh a\phi \ , \qquad V = -2W_0 \cosh b\phi \ . \tag{4.1}$$

A similar analysis could also be performed for other coupling functions as for instance $f(\phi) = 1 + \frac{\alpha}{2}\phi^2$. The action we consider is then

$$S = \int d^4x\sqrt{-g}\left[R - \frac{1}{2}(\partial\phi)^2 - \frac{f_0}{2}\cosh a\phi\, F^2 + 2W_0\cosh(b\phi) - 2\Lambda\right] \ , \tag{4.2}$$

where we included a negative cosmological constant $\Lambda < 0$. The radius of the AdS vacuum solution is

$$\frac{3}{L^2} = W_0 - \Lambda \ , \tag{4.3}$$

and stability of the vacuum requires that the parameter b satisfies the Breitenlohner-Freedman bound

$$b^2 \leq b_u^2 \ , \qquad b_u^2 \equiv \frac{3}{8}\left[1 - \frac{\Lambda}{W_0}\right] \ . \tag{4.4}$$

In this section we use the following parametrization for the metric

$$ds^2 = -\lambda(r)dt^2 + \frac{dr^2}{\lambda(r)} + H^2(r)(dx^2 + dy^2) \ . \tag{4.5}$$

The equation of motion of the gauge field can be immediately integrated and gives

$$A_0' = \frac{\rho}{fH^2} \ , \tag{4.6}$$

where ρ is the charge density of the solution. The remaining equations are

$$\begin{aligned}
(\lambda H^2)'' &= -2H^2\,(V + 2\Lambda) \ , \\
(H)'' &= -\frac{H}{4}(\phi')^2 \ , \\
(\lambda H^2\phi')' &= H^2\left[\frac{dV}{d\phi} - \frac{(A_0')^2}{2}\frac{df}{d\phi}\right] \ , \\
\lambda(H')^2 + \frac{\lambda'}{2}(H^2)' &= H^2\left[\frac{\lambda}{4}(\phi')^2 - \frac{f}{4}(A_0')^2 - \frac{V}{2} - \Lambda\right] \ .
\end{aligned} \tag{4.7}$$

The equation of motion of the scalar field contains an effective potential

$$\tilde{V}(\phi) = V(\phi) + \frac{\rho^2}{2H^4 f(\phi)} \ , \tag{4.8}$$

and one can find $AdS_2 \times \mathbb{R}^2$ solutions with constant $H = H_0$ and $\phi = \phi_0$ provided that

$$\frac{d\tilde{V}}{d\phi}(\phi_0) = 0 \ , \qquad \frac{\rho^2}{2H_0^4 f(\phi_0)} = -V(\phi_0) - 2\Lambda \ . \tag{4.9}$$

For the simple models discussed in this paper with potentials of the form given in (3.9), this is possible only if $m^2 > 0$ and for $\rho^2 a^2 > 4 f_0 m^2 H_0^4$. In this Section we will focus on models with $m^2 \leq 0$ and therefore we do not consider this possible class of solutions.

We will try instead the following scaling ansatz [22]

$$\lambda = \lambda_0 \, r^w (1 + p_1 \, r^\nu) \ , \qquad H = r^h (1 + p_2 \, r^\nu) \ , \qquad \phi = \phi_0 - \xi \ln r + p_3 \, r^\nu \ . \tag{4.10}$$

This scaling ansatz provides an exact solution to the equations of motion if the parameters are chosen in the following way

$$\xi = \frac{4(a+b)}{4 + (a+b)^2} \ , \qquad w = 2 - b\xi \ , \qquad h = \frac{(a+b)^2}{4 + (a+b)^2} \ , \tag{4.11}$$

$$\lambda_0 \ = \ \frac{2 W_0 e^{b\phi_0}}{(w+2h)(w+2h-1)} \ , \qquad \frac{\rho^2}{f_0} e^{-a\phi_0} = \frac{2 W_0 e^{b\phi_0}}{w+2h} (2 - 2h - b\xi) \ . \tag{4.12}$$

Using the previous relations we can express the parameter ϕ_0 in terms of the charge density and the other parameters of the model

$$\frac{\rho^2}{f_0} e^{-(a+b)\phi_0} = 2 W_0 \frac{2 - b(a+b)}{2 + b(a+b)} \ . \tag{4.13}$$

Finally the other parameters read

$$\begin{aligned} p_3 \ &= \ \frac{2 p_2}{\xi} (2h - 1 + \nu) \ , \\ p_1 (w + 2h + \nu)(w + 2h - 1 + \nu) \ &= \ p_3 b (w+2h)(w+2h-1) - 2 p_2 \left[\nu^2 + \nu (2w + 4h - 1) \right] \ , \end{aligned} \tag{4.14}$$

and the exponent ν is a real root of the following quartic equation

$$\begin{aligned} &Q(\nu) = (\nu + 1)(\nu + a\xi)(\nu^2 + A\nu + B) \ , \\ &A = 1 + \frac{2(a^2 - b^2)}{4 + (a+b)^2} \ , \quad B = -2A^2 + 2A \frac{(a+b)^2 (1 + ab)}{4 + (a+b)^2} \ . \end{aligned} \tag{4.15}$$

If we choose the greatest positive root the scaling ansatz describes the near-horizon region of the extreme black hole. It could be interesting to study the backgrounds corresponding to the other real roots of the polynomial (4.15). In Figure 6 we show the background fields obtained by integrating the near-horizon behavior discussed above up to infinity and requiring suitable boundary conditions.

The solution is extremal if $b\xi < 1$ which implies

$$b < b_e \ , \qquad b_e \equiv \frac{a}{3} \left[2 \sqrt{1 + \frac{3}{a^2}} - 1 \right] \ . \tag{4.16}$$

This condition together with the BF bound (4.4) restricts the possible value of b for a given value of a. When $b = 0$ the previous solution reduces to the solution found in [22] upon substituting W_0 with $2(W_0 - \Lambda)$. Since the extremal solution depends on the parameter b, it is not surprising that also the behavior of the conductivity at low frequencies is modified. As we will show in the next Section it vanishes as $\sigma(\omega) \sim \omega^{2 + \frac{b\xi}{1 - b\xi}}$.

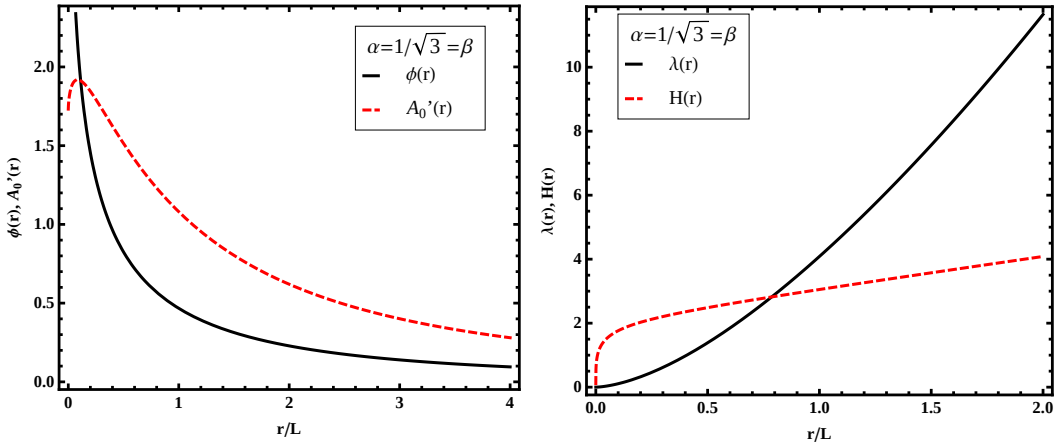

FIG. 6: Background fields at $T = 0$, Maxwell and scalar field (left) and metric functions (right).

The scaling ansatz in eq. (4.10) can also capture the near-horizon region of a near-extreme black hole [22]. The near-extreme solution corresponds to a negative value for the parameter $\nu = -\eta$ with

$$\eta = 1 + \frac{\xi}{2}(a - b) \ , \tag{4.17}$$

which implies $p_2 = p_3 = 0$. The parameters λ_0, ρ and φ_0 satisfy the relations already given in (4.12). The solution depends then on a parameter $p_1 \equiv -m$ and the metric is

$$ds^2 = \lambda_0 r^w \left(1 - \frac{m}{r^\eta}\right) dt^2 + \frac{dr^2}{\lambda_0 r^w \left(1 - \frac{m}{r^\eta}\right)} + r^{2-2h}(dx^2 + dy^2) \ . \tag{4.18}$$

The horizon radius is given by $r_0^\eta = m$. We will use this metric in Section V to clarify the low temperature behavior of the optical conductivity.

We note that since the scalar field diverges logarithmically as it approaches the extremal horizon, the same near-horizon analysis can be applied to the case of exponential coupling functions of the form $f(\phi) = f_0 e^{a\phi}$ and potentials of the form $V(\phi) = -W_0 e^{b\phi}$. Black hole solutions in Einstein-Maxwell-dilaton gravity with exponential coupling functions and Liouville-like potentials are discussed in [34–36].

V. HOLOGRAPHIC PROPERTIES OF THE NEW BLACK HOLE SOLUTION

The instability of the AdS-RN black hole towards developing a scalar hair signals a phase transition in the dual field theory defined on the boundary of AdS. When the scalar field is charged with respect to the $U(1)$ gauge field, in the dual theory there is a phase transition to a superfluid state characterized by the spontaneous breaking of a global $U(1)$ symmetry [12]. In our case the condensate is neutral and we have a phase transition between the state dual to the AdS-RN black hole and the state dual to the dilatonic black hole. As mentioned in the introduction, these two states have markedly different properties, in particular from the thermodynamical point of view.

In order to better illustrate the behavior of the new phase, we will display our results for the four models listed in the following table

	$f(\phi)$	$V(\phi)$	α	β
Model I	$\cosh(\sqrt{3}\phi)$	$-\frac{6}{L^2} - \frac{\phi^2}{L^2}$	3	-2
Model II	$1 + \frac{3}{2}\phi^2$	$-\frac{6}{L^2} - \frac{\phi^2}{L^2}$	3	-2
Model III	$\cosh(\sqrt{3}\phi)$	$-\frac{6}{L^2}\cosh\left(\frac{\phi}{\sqrt{3}}\right)$	3	-2
Model IV	$\cosh(10\phi)$	$-\frac{6}{L^2} - \frac{\phi^2}{L^2}$	100	-2

The first three models correspond to different choices for the coupling functions $f(\phi)$ and the potential $V(\phi)$ but they all have the same values for the parameters α and β that enter in the linear perturbation analysis of Section II.

The last model illustrates the behavior of the system for large values of the parameter α. As discussed in the previous Section, at low temperatures a simpler pattern appears: when the potential has the form given in (3.9) with $\beta \leq 0$ the properties of the model depend mainly on α and are affected by the presence of the potential only when this is an exponential function of the scalar field.

A. Phase transitions in the dual theory

Below T_c the new black hole solution develops a scalar hair and therefore the new phase of the dual theory is characterized by a scalar condensate. The temperature dependence of the expectation value of the neutral operator $\mathcal{O}_+$ or $\mathcal{O}_-$ can be determined using eq. (3.1) and the fact that the black hole temperature depends only on ϕ_h, the value of the scalar field at the horizon. In Figure 7 we display the scalar condensate at constant charge density and for different values of the temperature for our four models. The critical temperature is proportional to $\sqrt{\rho}$ where ρ is

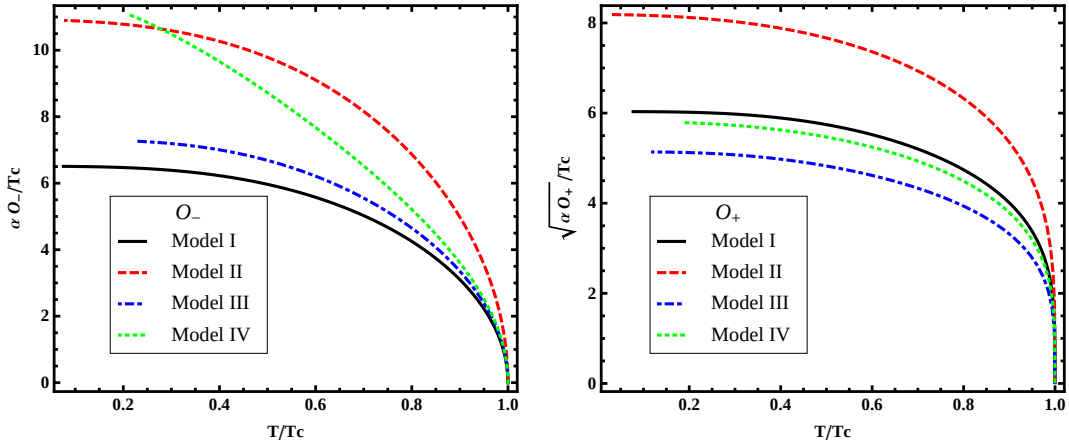

FIG. 7: Neutral condensate as a function of T for the two different boundary theories and for different models. Left: $\mathcal{O}_- \sim (1-T/T_c)^{1/2}$ near the critical temperature. Right: $\mathcal{O}_+ \sim (1-T/T_c)^{1/2}$ near the critical temperature.

the charge density. Near the critical temperature the scalar condensate behaves like $\sim (1-T/T_c)^{\gamma}$, with $\gamma = 1/2$ for both $\mathcal{O}_+$ and $\mathcal{O}_-$, which is the value of the exponent predicted by mean field theory [11, 37].

B. Electric conductivity in the dual theory

According to the AdS/CFT correspondence, transport phenomena in the dual field theory are related to linear perturbations of the equations of motion of the bulk fields. For instance the electric, thermal and thermoelectric conductivities can be derived from the equations governing the fluctuations of the component g_{tx} of the metric and A_x of the gauge field [6]. Perturbations of g_{tx} and A_x with zero spatial momentum and harmonic time dependence decouple from all the other modes and one is left with a system of just two equations

$$A_x'' + \left[\frac{g'}{g} - \frac{\chi'}{2} + \frac{1}{f(\phi)}\frac{df(\phi)}{d\phi}\phi'\right] A_x' + \frac{\omega^2}{g^2} e^{\chi} A_x = \frac{A_0' e^{\chi}}{g}\left[\frac{2}{r} g_{tx} - g_{tx}'\right], \tag{5.1}$$

$$g_{tx}' - \frac{2}{r} g_{tx} + A_0' A_x f(\phi) = 0\,. \tag{5.2}$$

Substituting the second equation in the first gives the following equation for the fluctuations of the gauge field

$$A_x'' + \left[\frac{g'}{g} - \frac{\chi'}{2} + \frac{1}{f(\phi)}\frac{df(\phi)}{d\phi}\phi'\right] A_x' + \left(\frac{\omega^2}{g^2} - \frac{{A_0'}^2 f(\phi)}{g}\right) e^{\chi} A_x = 0\,. \tag{5.3}$$

We solve eq. (5.3) with purely ingoing boundary conditions at the horizon. The electric, thermal and thermoelectric conductivities are given by [12]

$$\sigma = -i\frac{A_x^{(1)}}{\omega A_x^{(0)}}\,, \qquad \sigma_{te} = \frac{1}{T}\left(\frac{i\rho}{\omega} - \mu\sigma\right), \qquad \sigma_t = \frac{iM}{4\omega T}\,, \tag{5.4}$$

where $A_x^{(0)}$ and $A_x^{(1)}$ are fixed by the asymptotic behavior of the fluctuation at infinity

$$A_x \sim A_x^{(0)} + \frac{A_x^{(1)}}{r} \ . \tag{5.5}$$

In the following we will consider only the electric conductivity. Figures 8, 9 and 10 show its frequency dependence obtained by numerical integration of eq. (5.3).

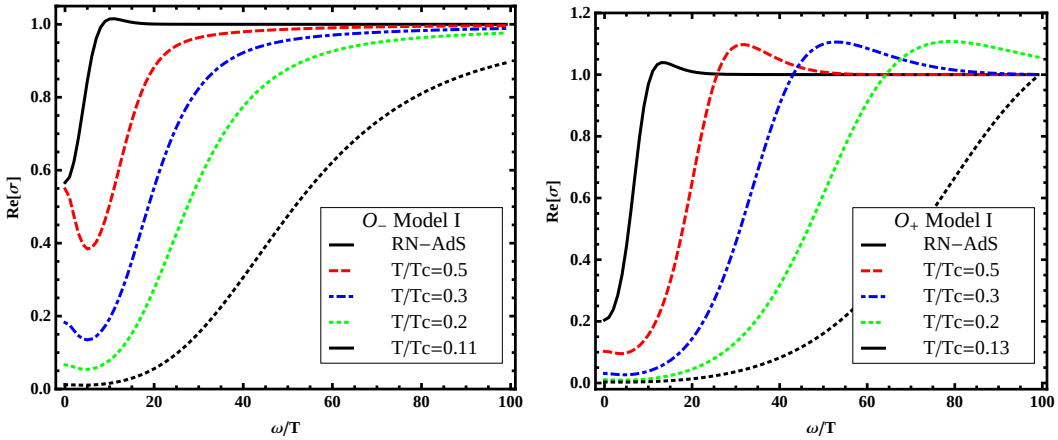

FIG. 8: Real part of the conductivity as a function of the frequency for different values of T and for the operators $\mathcal{O}_-$ (left) and $\mathcal{O}_+$ (right). We show results for Model I.

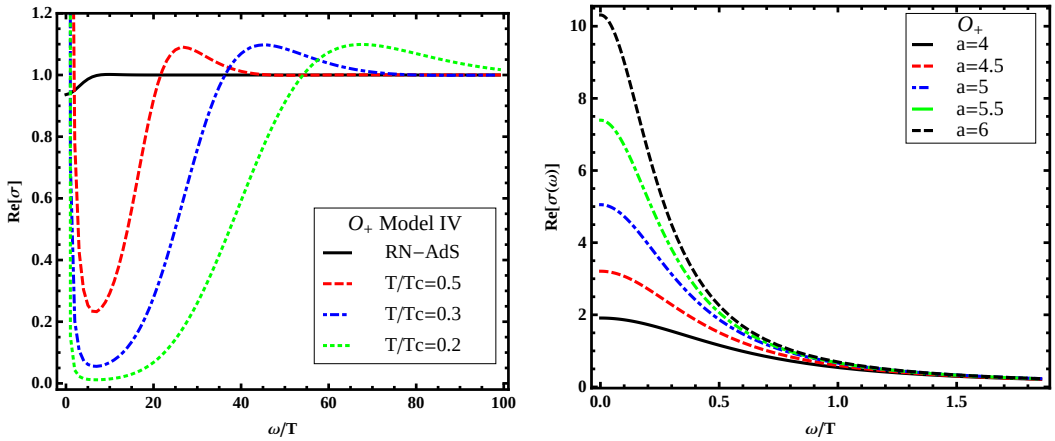

FIG. 9: Left: Real part of the conductivity as a function of the frequency for different values of T and for the operator $\mathcal{O}_+$. We show results for Model IV. Right: Real part of the conductivity for $\beta = -2$ and $f(\phi) = \cosh(a\phi)$ for increasing values of a.

The four models display similar qualitative features. In the high-frequency limit the real part of the conductivity becomes constant, a property common to every theory with an AdS_4 dual. Moreover, as a consequence of translation invariance, the imaginary part of σ has a simple pole at $\omega = 0$ and therefore the DC conductivity contains a delta function contribution at $\omega = 0$. The conductivity displays interesting behavior at small frequencies. From the plots we see that it develops a minimum and then it tends to a non-zero value as $\omega \to 0$, more pronounced for large values of the non-minimal coupling α, as shown in Fig. 9. This non-zero value of $\mathrm{Re}[\sigma]$ at $\omega = 0$ may be seen as an analogue of the Drude peak in the conductivity of ordinary metals. As we lower the temperature this additional contribution to the DC conductivity decreases and at zero temperature $\sigma(\omega)$ vanishes at low frequencies as a power with an exponent fixed by the geometry of the near-horizon region, as we will show below.

The frequency dependence of the conductivity is easier to understand if one rewrites Eq. (5.3) as a Schrödinger equation and expresses σ in term of a reflection coefficient [23]. In order to do so we introduce a new coordinate z

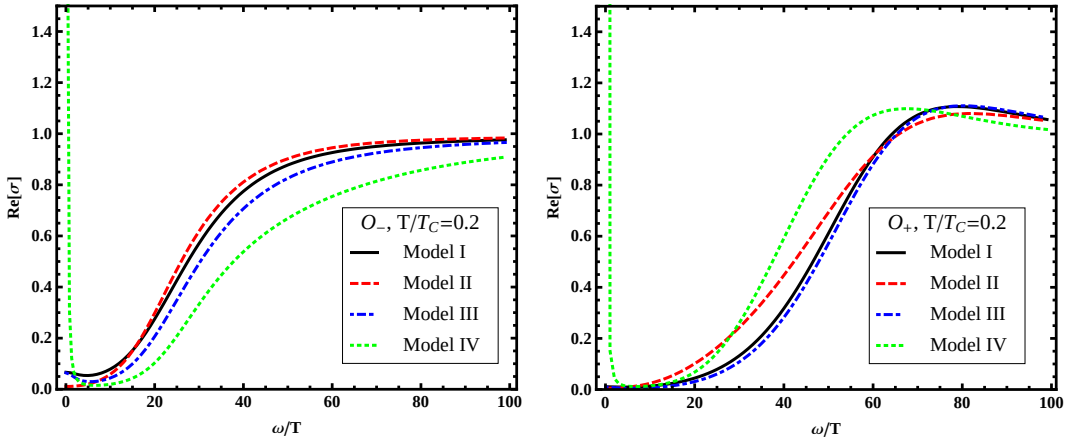

FIG. 10: Real part of the conductivity as a function of the frequency for different models at $T/T_c \sim 0.2$ and for the operators $\mathcal{O}_-$ (left) and $\mathcal{O}_+$ (right).

defined by

$$\frac{dr}{dz} = g e^{-\frac{\chi}{2}} \,, \tag{5.6}$$

and rescale the gauge field setting $\sqrt{f}A = \Psi$. In the new coordinates the horizon is at $z = -\infty$, the boundary of AdS at $z = 0$ and the field Ψ satisfies the following equation

$$\frac{d^2\Psi}{dz^2} + (\omega^2 - V(z))\Psi = 0 \,, \qquad V(z) = g f (A_0')^2 + \frac{1}{\sqrt{f}} \frac{d^2\sqrt{f}}{dz^2} \,. \tag{5.7}$$

The potential in Eq. (5.7) has two contributions. The second term is due to the non-minimal coupling, it is present also in the probe limit and it is always negative in the near-horizon region. The first term is always positive and corresponds to the backreaction of the metric.

To find solutions of the original problem with ingoing boundary conditions at the horizon it is convenient to extend the definition of the potential $V(z)$ to positive values of z by setting $V(z) = 0$ for $z > 0$. One then solves the one-dimensional Schrödinger equation with potential $V(z)$ for a particle incident on the potential barrier from the right [23]. For $z \geq 0$ the wave function is

$$\Psi(z) = e^{-i\omega z} + \mathcal{R} e^{i\omega z} \,, \qquad z \geq 0 \,, \tag{5.8}$$

where $\mathcal{R}$ is the reflection coefficient. Using Eq. (5.5) and (5.4) and the definition $\Psi = \sqrt{f}A$ one obtains

$$\sigma(\omega) = -\frac{i}{\omega} \frac{A_x^{(1)}}{A_0^{(0)}} = \frac{1-\mathcal{R}}{1+\mathcal{R}} - \frac{i}{2\omega} \left[\frac{1}{f} \frac{df}{dz} \right]_{z=0} \,. \tag{5.9}$$

The second term in the equation above contributes only to the imaginary part of the conductivity. When f starts with a term linear in ϕ this term vanishes for $\Delta > 1$, is constant for $\Delta = 1$ and diverges for $\Delta < 1$. When f starts with a term quadratic in ϕ and therefore satisfies the conditions in Eq. (2.4) it vanishes for $\Delta > 1/2$ and it is constant for $\Delta = 1/2$. The real part of the conductivity is completely determined by the reflection coefficient $\mathcal{R}$, hence by the form of the potential V in the Schrödinger equation.

The behavior of V at large r depends on the asymptotic expansion of the scalar field $\phi \sim O_\Delta / r^\Delta$ and on the coupling function $f(\phi)$. When f starts with a term linear in ϕ, as it is the case for $f = e^{a\phi}$, the potential is

$$V(z) \sim \rho^2 z^2 + \frac{a}{2} \Delta(\Delta - 1) O_\Delta (-z)^{\Delta - 2} \,, \tag{5.10}$$

and therefore it vanishes for $\Delta > 2$, is constant for $\Delta = 2$ and diverges for $1/2 < \Delta < 2$. When f starts with a term quadratic in ϕ, as it is the case for $f = \cosh(a\phi)$, the potential is

$$V(z) \sim \rho^2 z^2 + \frac{a^2}{2} \Delta(2\Delta - 1) O_\Delta^2 (-z)^{2(\Delta - 1)} \,, \tag{5.11}$$

and therefore it vanishes for $\Delta > 1$, is constant for $\Delta = 1$ and diverges for $1/2 < \Delta < 1$.

For non extremal black holes the potential tends to zero exponentially as the coordinate z tends to the horizon, $V(z) \sim V_h e^{4\pi T z}$ where T is the temperature of the black hole. While the potential of a model with a charged scalar minimally coupled to the gauge field is always positive, in our case the sign of the potential is not definite. Although it is always positive near the boundary, it can become negative and reach a minimum before vanishing at the horizon with a negative exponential tail. Whether the potential is positive or negative depends on the relative magnitude of the two terms in the Schrödinger potential, the one due to the non-minimal coupling and the one due to the backreaction. As we lower the temperature the effect of the backreaction becomes increasingly important. In fact at $T = 0$ the potential is always positive near the extremal horizon and vanishes like C/z^2, with a positive constant C.

The near-horizon behavior of the potential at $T = 0$ can be determined using the analytic form of the extremal solution found in the previous Section. With the form of the metric used in that Section the new coordinate z is given by

$$\frac{dr}{dz} = \lambda \ , \tag{5.12}$$

and the rescaled gauge field $\Psi = \sqrt{f} A$ satisfies the following equation

$$\frac{d^2\Psi}{dz^2} + (\omega^2 - V(z))\Psi = 0 \ , \qquad V(z) = \lambda f (A_0')^2 + \frac{1}{\sqrt{f}} \frac{d^2\sqrt{f}}{dz^2} \ . \tag{5.13}$$

Substituting the explicit form of the solution one obtains

$$V(z) = \frac{C}{z^2} \ , \qquad C = \frac{(2b\xi - 3)^2}{4(1 - b\xi)^2} - \frac{1}{4} \ . \tag{5.14}$$

Following the approach of [38] one can show that the optical conductivity vanishes at small frequencies and obtain an analytic expression for the leading power in ω by matching the conserved probability current of the Schrödinger equation near the boundary at infinity and near the horizon. The result is

$$\sigma(\omega) \sim \omega^{2 + \frac{b\xi}{1 - b\xi}} \ , \tag{5.15}$$

and this behavior is observed in our numerical results for the conductivity in the low temperature and low frequency limits.

The Schrödinger potential and the related conductivity are shown in Figs. 11. As mentioned before, also in this case there are several solutions to the field equations. The Schrödinger potential and the conductivity for these additional solutions can have several maxima and minima in the intermediate region between the horizon and infinity. These features are absent if the coupling function is exponential, $f \sim e^{a\phi}$.

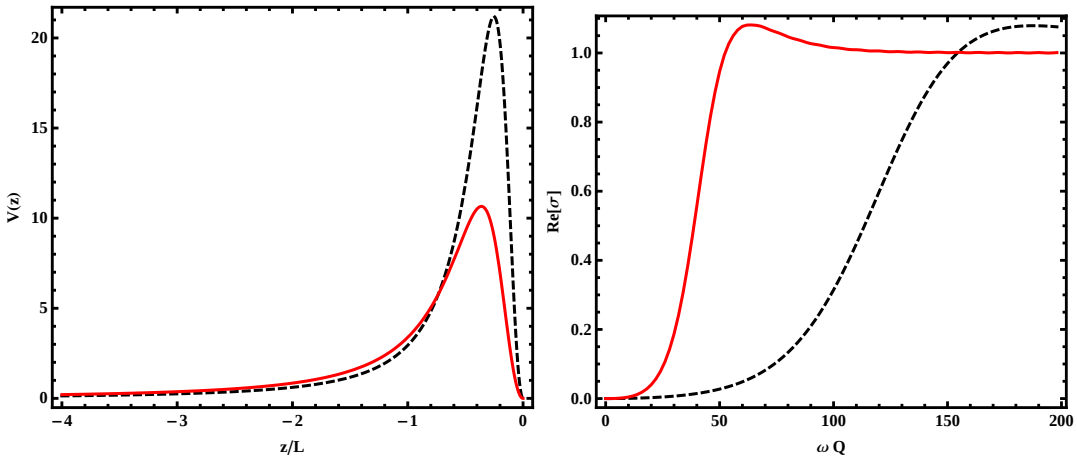

FIG. 11: Schrödinger potential (left) and electrical conductivity (right) at $T = 0$. Black dashed lines correspond to $b = 0$ and $a = 1$, whereas red straight lines correspond to $b = a = 1/\sqrt{3}$.

The other distinctive feature of the behavior of $\sigma(\omega)$, the presence of a peak at small frequencies when $T > 0$, is due to the fact that the potential of the Schrödinger problem is not positive definite and can support a resonance

near $\omega = 0$, causing a sharp increase in the DC conductivity. Using the near-extremal solution (4.18) we can clarify when to expect a peak in $\sigma(0)$ and when this peak will be present even at very low temperatures. The explicit form of the Schrödinger potential near the horizon is in this case

$$V(z) \sim \frac{A^2}{r_0}\left[2 - 2h - \left(b + \frac{a}{2}\right)\xi\right] e^{Az} \ , \tag{5.16}$$

where $A = \lambda_0 \eta r_0^{1-b\xi}$. The potential, as already observed, receives a negative contribution from the term due to the non-minimal coupling between the scalar and the gauge field and a positive contribution from the term due to the backreaction of the metric. From the previous expression we can see that the potential approaches zero with a negative exponential tail as $z \to -\infty$ if $a^2 + 2b^2 + 3ab > 4$. For a given b this happens for

$$a > \frac{1}{2}\left[\sqrt{b^2 + 16} - 3b\right] \ . \tag{5.17}$$

In particular when $b = 0$ this implies that the potential for the quasi-extreme black hole is positive near the horizon for $a < 2$ and negative for $a > 2$. In Figure 12 we display the potential for selected values of the temperature and the parameters to confirm that its behavior changes according to Eq. (5.17). When a negative exponential tail is present for the near-extremal solution, the value of the conductivity increases significantly at small frequencies even at low temperatures, as shown in Fig. 10. One can observe a small increase in $\sigma(\omega)$ at low frequencies even when the near-extremal potential is positive. This is due to the fact that at temperatures higher than those corresponding to the near-extremal black hole the term due to the non-minimal coupling can dominate the term due to the backreaction.

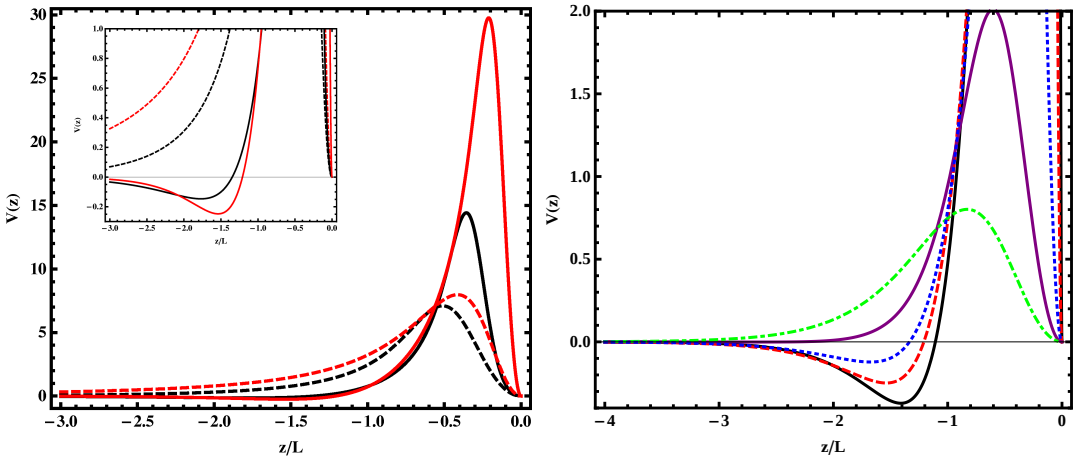

FIG. 12: Effective potential in eq. (5.7). Left: different models at fixed $T/T_c \sim 0.3$. Black lines refer to the case $b = 0$ and $a = 3$ (straight line) and $a = \sqrt{3}$ (dashed line). Red lines refer to $b = 1/\sqrt{3}$ and $a = \sqrt{3}$ (straight line) and $a = 1/\sqrt{3}$ (dashed line). According to eq. (5.17), straight and dashed lines correspond to potentials approaching $z = -\infty$ from below and above respectively, as shown in the inset. Right: the model $a = \sqrt{3}$ and $b = 1/\sqrt{3}$ for different temperature. From below to top $T/T_c \sim 0.2$, 0.3, 0.5, ,0.8, 1. The lower the temperature, the deeper the minimum.

A similar increase in $\sigma(\omega)$ at low frequencies was recently observed in models where the Born-Infeld action of a probe brane is coupled to a geometry with a Lifshitz scaling symmetry [24].

Another interesting feature of our model is that the DC conductivity $\sigma(0)$ depends in a non-monotonic way on the temperature, as shown in Fig. 13. This effect becomes more evident as the value of a increases. In terms of the resistivity Fig. 13 shows that there is a minimum at low temperature. A minimum in resistivity is observed in metals containing magnetic impurities and its presence was explained by Kondo as resulting from the interaction between the magnetic moment of the conduction electrons and the impurity. It would be interesting to identify in our model what kind of effective interaction is induced among the charge carriers by the scalar condensate which causes the minimum in resistivity.

VI. CONCLUSIONS

We have investigate a broad class of Einstein-Maxwell-dilaton gravity models in 4D AdS spacetime which admit both AdS-RN and charged dilatonic black hole solutions. Below a critical temperature the AdS-RN solution is unstable

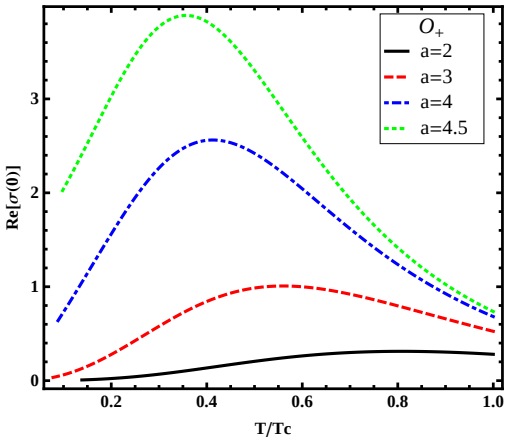

FIG. 13: DC conductivity for $V = -\frac{6}{L^2}\cosh(\phi/\sqrt{3})$ and $f = \cosh(a\phi)$. From bottom to top $a = 2$, 3, 4, 4.5.

and it undergoes a phase transition whose endpoint is the charged black hole dressed with a scalar field.

This instability is interesting from a purely gravitational perspective but it acquires a particular relevance when used in the context of the AdS/CFT correspondence to provide a holographic description of condensed matter phenomena. Our model describes a second order phase transition in the dual field theory in which a neutral scalar operator condenses below a critical temperature.

The new phase has interesting electric transport properties, presumably caused by the interactions of the charge carriers with the scalar condensate. When the temperature is not too close to zero, the optical conductivity has a minimum at low frequencies and then a "Drude peak", reaching a constant value at $\omega = 0$ which can be considerably larger than its constant value at high frequency. This effect is particularly evident for large values of the non-minimal coupling between the scalar and the gauge field. Another very interesting feature is that the resistivity does not increase monotonically with the temperature but displays a minimum. This effect is reminiscent of the Kondo effect, caused in real metal with magnetic impurities by the interactions of the magnetic moment of the conduction electrons with the magnetic moment of the impurity. It would be interesting to compute the precise temperature dependence of the resistivity and to clarify what kind of effective interaction causes the minimum in resistivity.

We also studied the extremal limit of the charged dilatonic black hole. The near-horizon metric has a Lifshitz scaling symmetry which is a simple generalization of the one found in [22]. Using the extremal solution we clarified the behavior of the numerical solutions in the zero temperature limit.

The analysis of the fluctuations of fermionic fields in the AdS-RN [39–43] and in the charged dilaton black hole background [17] provides evidence for the existence of a Fermi surface in the boundary theory. While in the former case the macroscopic ground state entropy prevents a simple interpretation of the dual phase, in the latter case one observes a more conventional behavior, with vanishing zero-point entropy and with a specific heat linear in the temperature. Since the phase transition discussed in this paper connects the AdS-RN and the charged dilatonic black hole, it may help to clarify the correct interpretation of the corresponding dual theories.

It would be interesting to study models which allow for both the instability studied in this paper and the instability caused by the minimal coupling of a charged scalar field. One could then investigate the effect of the neutral condensate on the properties of the superconducting phase. Our models can in fact be easily adapted to describe holographic superconductors by interpreting the scalar field as the modulus of a complex scalar and adding to the Lagrangian a coupling between the phase of the scalar and the gauge field. Models of this type were recently discussed in [44].

In order to identify precisely the dual theory and specify its operator content and Hamiltonian, it would be interesting to embed these black hole solutions into ten or eleven dimensional supergravity. For the holographic superconductors examples of this embedding were discussed in [45–48].

Appendix A: Scalar hairs in the probe limit. Schwarzschild-AdS background

Although in Sect. III we derived numerically the charged dilatonic black hole solution, it is of some interest to consider the regime in which one can neglect the back reaction of the matter fields on the gravitational field. The results of this Appendix can be compared with similar results obtained for the holographic superconductors in Ref.[12]. We shall follow closely the methods used in that paper, to which we refer for further details. We focus on potential

of the form $V(\phi) = -6/L^2 - \phi^2/L^2$. The outcome does not qualitatively change if one chooses a different V as long as Eq. (2.4) is satisfied. The limit in which the dynamics for the scalar and electromagnetic field decouples from the gravitational dynamics is obtained for $\alpha \to \infty$, after the rescaling $\phi \to \phi/\alpha$ and $A_0 \to A_0/\alpha$. The gravitational part of the dynamics, represented by the sourceless Einstein equations, is solved by the planar AdS-Schwarzschild (AdS-S) background

$$ds^2 = -g(r)dt^2 + \frac{dr^2}{g(r)} + r^2(dx^2 + dy^2)\,, \tag{A1}$$

with $g(r) = r^2/L^2 - 2M/r$. The black hole horizon is located at $r_h = (2ML^2)^{1/3}$, and the temperature is given by $T = \frac{3(2M)^{1/3}}{4\pi L^{4/3}}$. After using eq. (4.6) the dynamics for the scalar field is described by a single equation

$$\phi''(r) + \left[\frac{2}{r} + \frac{g'}{g}\right]\phi'(r) + \frac{1}{g}\left(\frac{\rho^2}{2r^4}\frac{1}{f(\phi)^2}\frac{df}{d\phi} - \frac{dV}{d\phi}\right) = 0\,, \tag{A2}$$

which has to be numerically integrated. The numerical integration is performed using the method explained in Sect. III. Setting either $\mathcal{O}_- = 0$ or $\mathcal{O}_+ = 0$ in eq. (3.1), we find a one-parameter family of solutions. Varying the single free parameter ϕ_h we obtain the condensate as a function of the temperature T/T_c. Numerical results are shown in Figure 14 and they represent the $\alpha \gg 1$ limit of the exact solution described in the main text. We plot the results

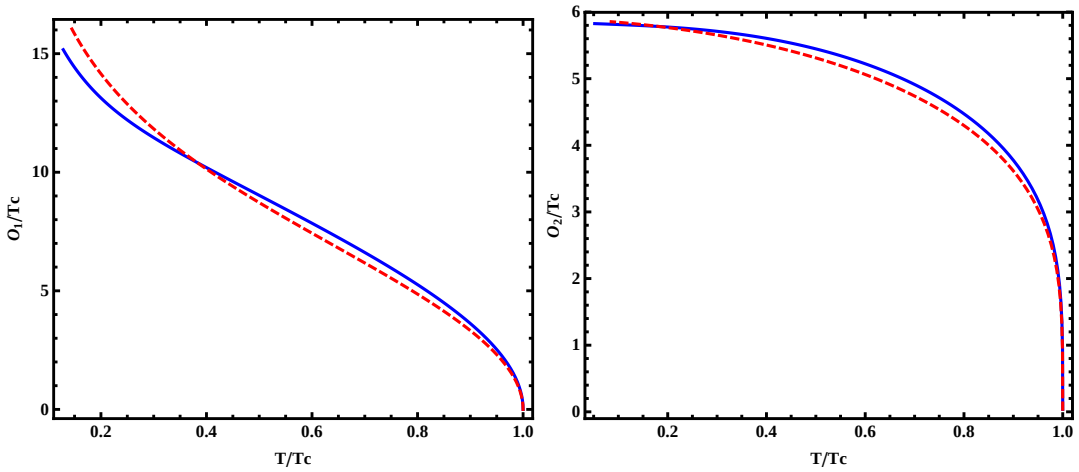

FIG. 14: Condensate of the scalar operator as a function of the temperature for $\mathcal{O}_-$ (left) e $\mathcal{O}_+$ (right). Straight blue line is $f(\phi) = \cosh(\phi)$ and dashed red line is $f(\phi) = 1 + \phi^2/2$. In both cases the potential is $L^2V(\phi) = -6 - \phi^2$. For the two operators we have $T_c \sim 0.182\sqrt{\rho}$ and $T_c \sim 0.135\sqrt{\rho}$ respectively.

for two different choices of the coupling functions: $f(\phi) = \cosh(\phi)$ and $f(\phi) = 1 + \phi^2/2$. The condensate $\mathcal{O}_-$ diverges as $T \to 0$. The divergence is an artifact of the probe limit approximation and it is removed once the backreaction is taken into account, as shown in Figure 7.

We conclude with a brief discussion of the conductivity in the probe limit. The perturbation equation reads

$$A_x''(r) + \left(\frac{g'}{g} + \frac{1}{f(\phi)}\frac{df(\phi)}{d\phi}\phi'\right)A_x'(r) + \frac{\omega^2}{g^2}A_x(r) = 0\,. \tag{A3}$$

Using the AdS/CFT definition (5.4) we obtain the results shown in Figure 15 for the real and imaginary part of the conductivity and for the condensate $\mathcal{O}_+$. Similar results are obtained for $\mathcal{O}_-$. The increase of $\sigma(\omega)$ at low frequencies, typical of the dilaton black holes considered in this paper, is evident in the probe limit. In fact it grows exponentially as $T/T_c \to 0$ but this is an artifact of the probe limit and disappears once the back reaction is taken into account (see Fig. 8). Finally, since translation invariance is broken by the AdS-S background, the imaginary part does not have a pole but vanishes for $\omega \to 0$. From the dispersion relations it follows that the DC conductivity is finite at $\omega = 0$ in the probe limit.

[1] J. M. Maldacena, Adv. Theor. Math. Phys. **2**, 231 (1998), hep-th/9711200.

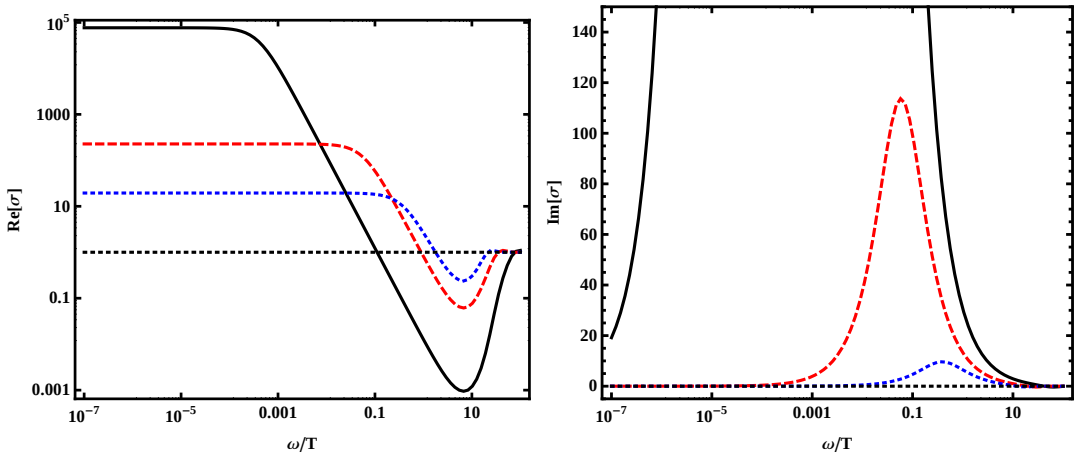

FIG. 15: Real (left) and imaginary (right) part of the conductivity in a log scale for $\mathcal{O}_+$ and $f(\phi) = \cosh(\phi)$. $T/T_c \sim 0.14\,, 0.3\,, 0.5\,, 1$ from bottom to top.

[2] D. T. Son and A. O. Starinets, Ann. Rev. Nucl. Part. Sci. **57**, 95 (2007), 0704.0240.
[3] D. Mateos, Class. Quant. Grav. **24**, S713 (2007), 0709.1523.
[4] S. Sachdev and M. Mueller (2008), 0810.3005.
[5] C. P. Herzog, J. Phys. **A42**, 343001 (2009), 0904.1975.
[6] S. A. Hartnoll (2009), 0903.3246.
[7] J. McGreevy (2009), 0909.0518.
[8] D. T. Son and A. O. Starinets, JHEP **09**, 042 (2002), hep-th/0205051.
[9] W. Israel, Phys. Rev. **164**, 1776 (1967).
[10] S. S. Gubser and S. S. Pufu, JHEP **11**, 033 (2008), 0805.2960.
[11] S. A. Hartnoll, C. P. Herzog, and G. T. Horowitz, JHEP **12**, 015 (2008), 0810.1563.
[12] S. A. Hartnoll, C. P. Herzog, and G. T. Horowitz, Phys. Rev. Lett. **101**, 031601 (2008), 0803.3295.
[13] G. W. Gibbons and K.-i. Maeda, Nucl. Phys. **B298**, 741 (1988).
[14] D. Garfinkle, G. T. Horowitz, and A. Strominger, Phys. Rev. **D43**, 3140 (1991).
[15] S. Monni and M. Cadoni, Nucl. Phys. **B466**, 101 (1996), hep-th/9511067.
[16] M. J. Duff and J. T. Liu, Nucl. Phys. **B554**, 237 (1999), hep-th/9901149.
[17] S. S. Gubser and F. D. Rocha (2009), 0911.2898.
[18] S. S. Gubser, Class. Quant. Grav. **22**, 5121 (2005), hep-th/0505189.
[19] S. S. Gubser and I. Mitra (2000), hep-th/0009126.
[20] S. A. Hartnoll and C. P. Herzog, Phys. Rev. **D77**, 106009 (2008), 0801.1693.
[21] S. Kachru, X. Liu, and M. Mulligan, Phys. Rev. **D78**, 106005 (2008), 0808.1725.
[22] K. Goldstein, S. Kachru, S. Prakash, and S. P. Trivedi (2009), 0911.3586.
[23] G. T. Horowitz and M. M. Roberts (2009), 0908.3677.
[24] S. A. Hartnoll, J. Polchinski, E. Silverstein, and D. Tong (2009), 0912.1061.
[25] P. Breitenlohner and D. Z. Freedman, Phys. Lett. **B115**, 197 (1982).
[26] G. Dotti and R. J. Gleiser, Class. Quant. Grav. **22**, L1 (2005), gr-qc/0409005.
[27] E. Berti, V. Cardoso, and A. O. Starinets, Class. Quant. Grav. **26**, 163001 (2009), 0905.2975.
[28] S. Mignemi (2009), 0907.0422.
[29] I. Z. Stefanov, S. S. Yazadjiev, and M. D. Todorov, Mod. Phys. Lett. **A23**, 2915 (2008), 0708.4141.
[30] G. T. Horowitz and M. M. Roberts, Phys. Rev. **D78**, 126008 (2008), 0810.1077.
[31] I. R. Klebanov and E. Witten, Nucl. Phys. **B556**, 89 (1999), hep-th/9905104.
[32] T. Hertog and G. T. Horowitz, JHEP **07**, 073 (2004), hep-th/0406134.
[33] M. Ammon, J. Erdmenger, M. Kaminski, and P. Kerner, JHEP **10**, 067 (2009), 0903.1864.
[34] R.-G. Cai and Y.-Z. Zhang, Phys. Rev. **D54**, 4891 (1996), gr-qc/9609065.
[35] R.-G. Cai, J.-Y. Ji, and K.-S. Soh, Phys. Rev. **D57**, 6547 (1998), gr-qc/9708063.
[36] C. Charmousis, B. Gouteraux, and J. Soda, Phys. Rev. **D80**, 024028 (2009), 0905.3337.
[37] K. Maeda, M. Natsuume, and T. Okamura, Phys. Rev. **D79**, 126004 (2009), 0904.1914.
[38] S. S. Gubser and F. D. Rocha, Phys. Rev. Lett. **102**, 061601 (2009), 0807.1737.
[39] S.-J. Rey, Prog. Theor. Phys. Suppl. **177**, 128 (2009), 0911.5295.
[40] S.-S. Lee, Phys. Rev. **D79**, 086006 (2009), 0809.3402.
[41] H. Liu, J. McGreevy, and D. Vegh (2009), 0903.2477.
[42] M. Cubrovic, J. Zaanen, and K. Schalm (2009), 0904.1993.

[43] T. Faulkner, H. Liu, J. McGreevy, and D. Vegh (2009), 0907.2694.
[44] F. Aprile and J. G. Russo (2009), 0912.0480.
[45] J. P. Gauntlett, J. Sonner, and T. Wiseman, Phys. Rev. Lett. **103**, 151601 (2009), 0907.3796.
[46] S. S. Gubser, S. S. Pufu, and F. D. Rocha (2009), 0908.0011.
[47] S. S. Gubser, C. P. Herzog, S. S. Pufu, and T. Tesileanu, Phys. Rev. Lett. **103**, 141601 (2009), 0907.3510.
[48] J. Gauntlett, J. Sonner, and T. Wiseman (2009), 0912.0512.